Earth Planets Space, **61**, 1297–1312, 2009

Nonstationary ray decomposition in a homogeneous half space

Shigeo Kinoshita

Yokohama City University, Seto 22-2, Kanazawa-ku, Yokohama 236-0027, Japan

(Received November 7, 2008; Revised July 20, 2009; Accepted August 26, 2009; Online published January 18, 2010)

A method for decomposing an *SH*-wave at the surface into the instantaneous power of shearing strain associated with rays in a homogeneous half space as a function of lapse time t and depth time τ, which is the travel time for the depth direction, is demonstrated. The instantaneous power in the (t, τ) space shows local maxima at the intersections of up-coming and down-going rays, which correspond to the velocity boundaries of the real layered structure beneath the site. Thus, the proposed method provides a tool for estimating the velocity boundaries of real layered structure from only surface recordings. The estimated results obtained by applying the proposed method to strong-motion data recorded at two Kanto sediment sites are in good agreement with the velocity boundaries previously determined by means of down-hole methods.

Key words: Ray decomposition, Wigner-distribution, instantaneous power, velocity discontinuity.

1. Introduction

Seismic signals are nonstationary time series. This nonstationarity is due to the nonstationarity of the fault rupture process itself emitting seismic waves and due to modulation effects that occur along the propagation paths, which generate various transient phases. This limits the application of Fourier analysis and second-order stationary time series analyses, such as correlation or spectral analyses, to seismic signals. Similarly, the constituent components of a wave (e.g., phase and energy) propagating along a ray are nonstationary signals. Thus, in order to investigate the time-dependent behavior of seismic waves (e.g., constructive or destructive interference) generated inside a layered medium, the nonstationarity of constituent components of the seismic wave associated with rays must be considered.

In the present study, representation and estimation methods of the instantaneous power of traveling waves associated with rays in a multi-layered structure are performed. The instantaneous power is represented as a function of lapse time t and depth time τ, which is defined as the travel time of the wave associated with a ray, from the surface in the depth direction. This (t, τ)-type nonstationary representation of instantaneous power for a multi-layered structure is calculated in terms of the Wigner-Ville distribution (Claasen and Mecklenbrauker, 1980a), and the (t, τ)-type representation is estimated for a homogeneous half space using seismograms recorded at the surface. This means that the surface recordings are decomposed into the intrinsic seismic waves associated with rays in terms of the instantaneous power in the (t, τ) space, which is demonstrated as nonstationary ray decomposition. Despite the ray decomposition into the homogeneous half space, this nonstationary ray decomposition preserves a portion of the characteristics of the instantaneous power in the (t, τ) space for the multi-layered structure, showing the local maxima (or minima) of instantaneous power at the intersections of up-coming and down-going rays. This important fact concerning the local maxima (or minima) of instantaneous power provides information for the detection of velocity boundaries in a layered medium.

As an example of the application of nonstationary ray decomposition to seismograms recorded at the surface, the velocity boundaries in a structure composed of a thick sedimentary deposit having a thickness of several kilometers overlying the pre-Tertiary basement, i.e., a sedimentary layer-basement system, are estimated. This is a direct application of nonstationary ray decomposition. In the present study, the estimated results at two Kanto sediment sites, the FCH and YKH stations, are in good agreement with the real structures previously obtained by the down-hole method (Yamamizu *et al.*, 1980; Yamamizu, 2004). Hence, the nonstationary ray decomposition method provides a tool for the estimation of travel times from the surface to the major velocity boundaries in the sedimentary layer-basement system.

In the proposed method, a seismic signal is interpreted as a nonstationary stochastic process, rather than a second-order stationary process. In the second-order process, the first- and second-order moments of the time series are time-independent, so that the auto-covariance function is a function of only the delay time. By removing the constraint of second-order stationarity from the seismic signal, methods for reinterpreting the seismic signal are constructed. For example, using the time-dependent first-order moment of the seismic signal, tilt motions are estimated from the strong-motion seismograms recorded in near-source regions (Kinoshita, 2008b; Kinoshita *et al.*, 2009). In the present article, using the auto-covariance function as a func-

tion of both lapse time and delay time, each phase on the seismogram is shown to be mapped onto a ray traveling in a homogeneous half space, so that the estimation of velocity discontinuities in a velocity structure beneath a site becomes possible. In a similar study, one-dimensional seismic interferometry was used to find the velocity discontinuities in a velocity structure beneath a site (Claerbout, 1968; Nakahara, 2006). Seismic interferometry assumes a second-order stationary process for seismic signals and uses the auto-covariance function of the seismic signal as a function of only delay time. The difference between the auto-covariance function used in seismic interferometry and that used in the proposed method is described in the Method section.

2. Method

In decomposing the *SH*-wave recorded at the surface into its intrinsic waves associated with rays, the rays are represented as a function of lapse time t and depth time τ in a homogeneous half space, as described in Introduction. The intrinsic wave is denoted by $x(t,\tau)$ and is measured by the instantaneous power $|x(t,\tau)|^2$. This decomposition is demonstrated through the following three steps. First, the instantaneous power $|x(t,\tau)|^2$ is calculated for a multi-layered model using an equal-time layered model. Next, the estimation method of instantaneous power $|x(t,\tau)|^2$ using surface recordings is constructed, given that the rays are represented in the (t,τ) space for the homogeneous half space. Finally, from the difference between the calculated and estimated instantaneous powers, the basic characteristics of the instantaneous power estimated using the nonstationary ray decomposition method are discussed.

2.1 Ray decomposition for the equal-time layered model

First, we consider the response of the Goupillaud-type layered medium (Goupillaud, 1961), i.e., an equal-time layered model, for an *SH*-wave. The equal-time layered model is a kind of multi-layered model composed of fine layers: each layer has a common travel time across a layer, i.e., $\Delta T/2$, where ΔT is the sampling time of seismic data. Thus, the transfer functions of the equal-time layered model are constructed in the z-transform domain using a frequency parameter $\lambda = 2\pi f\cdot\Delta T = \omega\cdot\Delta T$, ($|\lambda|\le\pi$ and f in Hz). Equal-time layered models depend on the ray incidence angle in the deepest layer. The equal-time layered model is an approximate model for real media. Given that the model has p layers that overlie a half space, i.e., the $(p+1)$th layer, the reflection coefficient of the up-coming wave at the top of the $(n+1)$th layer is given by

$$\kappa_n = \frac{\rho_{n+1}V_{n+1}\cos\phi_{n+1} - \rho_n V_n\cos\phi_n}{\rho_{n+1}V_{n+1}\cos\phi_{n+1} + \rho_n V_n\cos\phi_n}, \tag{1}$$

where ρ_n, V_n, and ϕ_n are the mass density, the S-wave velocity, and the angle of incidence in the nth layer, respectively. Using relation (1), the z transforms of the up-coming and down-going waves at the top of the $(n+1)$th layer, are shown for the incidence wave, $z^{-1/2}\hat{X}_{p+1}(\lambda)$, in the $(p+1)$th layer, respectively, as (Kinoshita, 1981, 1999):

$$\begin{aligned} z^{-\frac{1}{2}}\hat{X}_{n+1}(\lambda) &\equiv \left(\frac{s_p}{s_n}\right)\frac{z^{-\frac{p-n}{2}}\sum_{k=0}^{n}a_k^{(n)}z^{-k}}{\sum_{k=0}^{p}a_k^{(p)}z^{-k}}z^{-\frac{1}{2}}\hat{X}_{p+1}(\lambda) \quad\text{and}\\ \tilde{X}_{n+1}(\lambda) &\equiv \left(\frac{s_p}{s_n}\right)\frac{z^{-\frac{p+n}{2}}\sum_{k=0}^{n}a_k^{(n)}z^{k}}{\sum_{k=0}^{p}a_k^{(p)}z^{-k}}z^{-\frac{1}{2}}\hat{X}_{p+1}(\lambda) \end{aligned} \tag{2}$$

where the auto-regression coefficients $\{a_k^{(n)}\}_{k=1,2,\ldots,n-1}$, $(n=1,2\ldots,p)$ are calculated from the Levinson recursion (Levinson, 1947):

$$\begin{aligned} &a_n^{(n)} = \kappa_n, \quad a_0^{(n)} = 1, \quad n = 1,2,\ldots,p\\ &a_k^{(n)} = a_k^{(n-1)} + a_n^{(n)}a_{n-k}^{(n-1)}, \quad k = 1,2,\ldots,n-1. \end{aligned} \tag{3}$$

In relation (3), reflection coefficients $\{\kappa_n\}_{n=1}^{p}$ are referred to as the partial auto-correlation coefficients, and the gain factors are given by

$$s_n = 2\sum_{k=0}^{n}a_k^{(n)} = \prod_{k=0}^{n}(1+\kappa_k), \quad n = 1,2,\ldots,p. \tag{4}$$

In relation (2), the z variable is defined as $z = \exp(i\lambda)$. Furthermore, two types of waves associated with the rays in the z domain are defined as follows:

$$X_{n+1}^{(\pm)}(\lambda) = z^{-\frac{1}{2}}\hat{X}_{n+1}(\lambda) \pm \tilde{X}_{n+1}(\lambda), \tag{5}$$

where the superscript $+$ indicates an ordinary elastic wave, such a velocity wave, that is observable by a borehole seismometer installed in the $(n+1)$th layer, and the superscript $-$ indicates a shearing strain wave (or stress wave) multiplied by $2V_{n+1}$ that is not observable by the borehole seismometer. Thus, the transfer functions of these waves in the nth layer for an incidence wave $z^{-1/2}\hat{X}_{p+1}(\lambda)$ in the $(p+1)$th layer are given by

$$X_n^{(\pm)}(\lambda)\Big/z^{-\frac{1}{2}}\hat{X}_{p+1}(\lambda). \tag{6}$$

Using relations (2) and (5), the time series of these waves in the nth layer, $\{x_n^{(\pm)}(k\Delta T)\}$ are calculated using the time series of the incidence velocity wave, $z^{-1/2}\hat{X}_{p+1}(\lambda)$. Then, the instantaneous power of $x_n^{(\pm)}(k\Delta T)$ is given by

$$\left|x_n^{(\pm)}(k\Delta T)\right|^2 = \frac{1}{2\pi}\int_{-\pi/2}^{\pi/2}W_{x(\pm)}(k\Delta T,\lambda;n)d\lambda \tag{7}$$

(Claasen and Mecklenbrauker, 1980b). In this relation, $W_{x(\pm)}(k\Delta T,\lambda;n)$ is the discrete Wigner-Ville distribution of $x_n^{(\pm)}(k\Delta T)$, which is defined as follows:

$$\begin{aligned} W_{x(\pm)}(k\Delta T,\lambda;n) \equiv &\sum_{l=-\infty}^{\infty}2x_n^{(\pm)}((k+l)\Delta T)\\ &\cdot\left[x_n^{(\pm)}((k-l)\Delta T)\right]^* e^{-i2l\lambda}, \end{aligned} \tag{8}$$

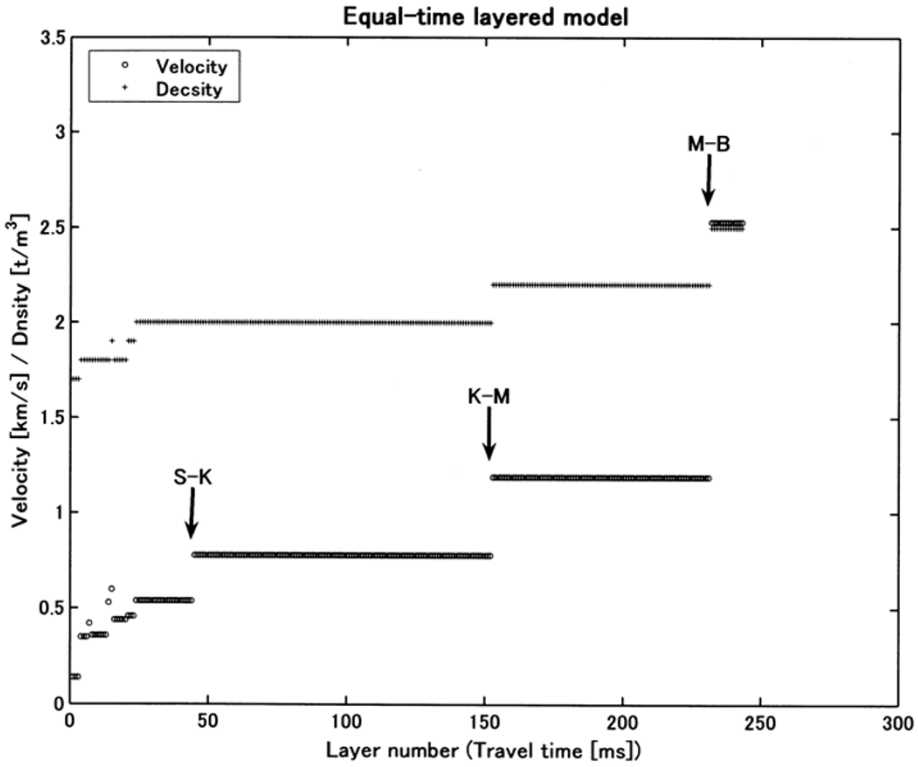

Fig. 1. Equal-time layered model beneath the FCH site for an incidence angle of 30°.

where "*" indicates a complex conjugation. Relation (7) is obtained from the inverse transform of the Wigner-Ville distribution as follows:

$$2x_n^{(\pm)}((k+l)\Delta T)\left[x_n^{(\pm)}((k-l)\Delta T)\right]^* = \frac{1}{2\pi}\int_{-\pi}^{\pi} W_{x(\pm)}\left(k\Delta T, \frac{\lambda}{2}; n\right) e^{il\lambda} d\lambda. \quad (9)$$

According to the definition of the Wigner-Ville distribution, $W_{x(\pm)}(k\Delta T, \lambda; n)$ is easily calculated using the fast Fourier transform, as follows:

$$W_{x(\pm)}\left(k\Delta T, \lambda = \frac{m\pi}{M}; n\right) \equiv \sum_{l=-N+1}^{N-1} 2x_n^{(\pm)}((k+l)\Delta T)\left[x_n^{(\pm)}((k-l)\Delta T)\right]^* e^{-il\frac{2m\pi}{M}}, \quad (10)$$

where $M = 2N - 1$. In the present study, the data length, $2M\Delta T$, is used in the calculation of the Wigner-Ville distribution. Thus, the range of lapse time parameter k is $1 \le k \le 2M$. The square root of the instantaneous power may correspond to the root-mean-square (RMS) value of $x_n^{(\pm)}(k\Delta T)$. In the present study, the Wigner-Ville distribution $W_{x(\pm)}(k\Delta T, \lambda; n)$ is actually calculated using the analytic signal of the real valued seismogram, $x_n^{(\pm)}(k\Delta T)$, which is obtained as follows:

$$x_n^{(\pm)}(k\Delta T) + iH\left[x_n^{(\pm)}(k\Delta T)\right]. \quad (11)$$

An analytic signal is used to prevent the aliasing effects of negative Fourier components of the real-valued signal and to suppress the cross term of the Wigner-Ville distribution at low frequencies (Claasen and Mecklenbrauker, 1980a). In relation (11), $H[x(k\Delta T)]$ is the Hilbert transform of $x(k\Delta T)$. The integrand $W_{x(\pm)}(k\Delta T, \lambda; n)$ of relation (7) is the Wigner transform of waves associated with the rays in the nth layer, and the left-hand side of relation (7) shows the instantaneous power of the waves as a function of the parameter set (k, n). Thus, introducing the transforms of the parameters, $t = k\Delta T$ and $\tau = n\Delta T/2$, relation (7) becomes a (t, τ)-type representation of the instantaneous power of the wave associated with the rays in the nth layer. This representation is the key "measurement" in the present study and is referred to hereinafter as the (t, τ)-representation of the ray.

Next, an example of the (t, τ)-representation of a ray is shown. Hereinafter, the $x_n^{(-)}(k\Delta T)$ wave, i.e., the velocity normalized strain wave, is considered. Assuming that a Ricker wave packet with a center period of T_o is an incidence wavelet, the (t, τ)-representation of the ray for a sedimentary layer-basement system at the FCH (Fuchu) station is calculated. The velocity structure beneath the FCH site was investigated using the down-hole method (Yamamizu *et al.*, 1980). Figure 1 shows the equal-time layered model at the site for an incidence angle of 30°. Figure 2 shows a simulated velocity seismogram at the surface for the Ricker wave with $T_o = 1/3$ s. Using relations (2), (5), and (7), the (t, τ)-representation of the ray is calculated as shown in Fig. 3. In Fig. 3 and following figures, the normalized square root of instantaneous power given in relation (7) is plotted rather than the instantaneous power itself. In this simulation, the S-wave attenuation $Q(f) = 50f$ ob-

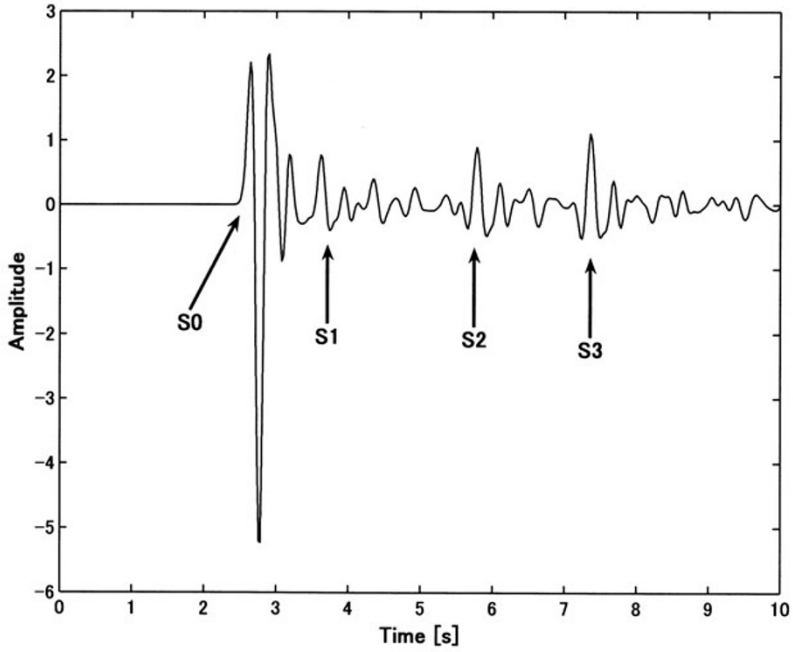

Fig. 2. Surface seismogram calculated for the equal-time layered model shown in Fig. 1 using $Q(f) = 50f$, where f is the frequency in Hz. The input wave is a Ricker wavelet with a central period of 1/3 s.

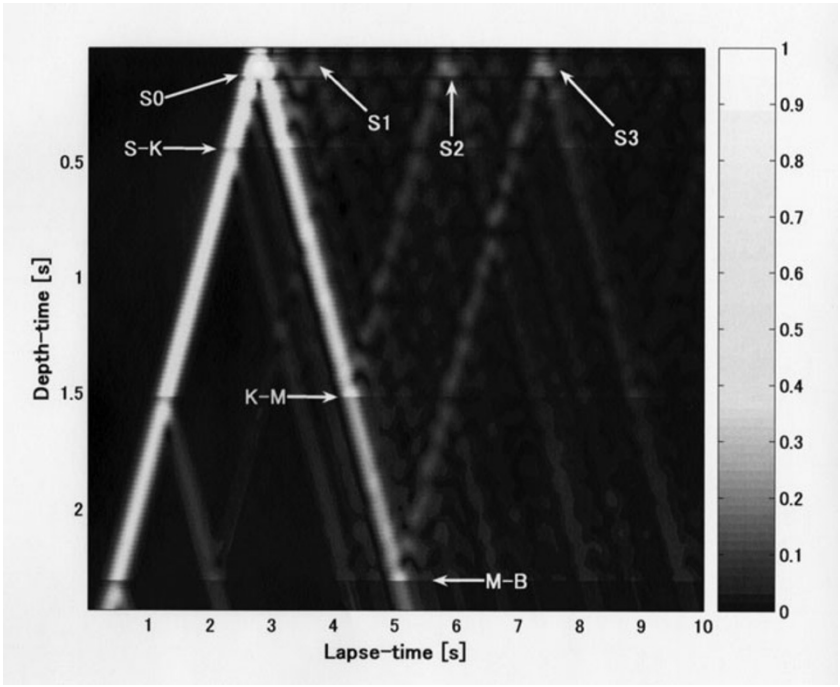

Fig. 3. Normalized root mean square of instantaneous power calculated from the equal-time layered model shown in Fig. 1 using $Q(f) = 50f$, where f is the frequency in Hz, and the input wave is a Ricker wavelet with a central period of 1/3 s.

tained by Kinoshita (2008a) at the FCH site for frequencies lower than approximately 3 Hz and a frequency transformation for introducing attenuation into the sedimentary layer-basement system (Kobori and Minai, 1969) are used. Comparing the (t, τ)-representation of the ray in Fig. 3 with the simulated wave shown in Fig. 2, reveals three phases reflected at the top of pre-tertiary basement (K-B boundary in Fig. 1) and two major boundaries in the sediment, which are the boundaries denoted by S-K and K-M in Fig. 1. The most important consideration is the appearance of local maxima of instantaneous power in the (t, τ)-representation of the ray, which are located at the intersections of up-coming and down-going rays, i.e., the boundaries of velocity structure at the site, as shown in Fig. 1. In addition to the local maxima, the discontinuity of instantaneous power at the boundaries is observed in Fig. 3, although this characteristic disappears

in the (t, τ)-representation of the ray estimated for the homogeneous half space model, as described in the following discussion.

2.2 Nonstationary ray decomposition of a strain wave for a homogeneous half space

Since the surface seismograms have characteristic information described by the (t, τ)-representation of the ray defined by relation (7) for a layered medium, the procedure for estimating the instantaneous power of the strain wave associated with rays in a homogeneous half space as a function of lapse time and depth time must be developed using surface recordings only. To develop this estimation procedure, the following three assumptions are needed: 1) the ray is decomposed in a homogeneous half space medium with an S-wave velocity of V, 2) the vertical axis is in the depth direction, and 3) surface recordings are velocity seismograms, $v(t)$. Based on these assumptions, the shearing strain at a depth of h is given by summing the up-coming and down-going waves of the shearing strain:

$$\varepsilon(t, h) \equiv \frac{1}{2V} v\left(t + \frac{h}{V}\right) + \frac{(-1)}{2V} v\left(t - \frac{h}{V}\right). \quad (12)$$

Thus, the cross-covariance function of up-coming and down-going waves of shearing strain is given by

$$\frac{-1}{4V^2} \int v\left(t + \frac{\tau}{2}\right) v\left(t - \frac{\tau}{2}\right) dt \equiv \frac{-1}{4V^2} R_V(\tau), \quad (13)$$

where $\tau = 2h/V$ is the lag-time. This means that the cross-covariance function between up-coming and down-going waves of shearing strain in a homogeneous half space is the auto-covariance function $R_V(\tau)$ of the velocity wave recorded at the surface multiplied by a factor of $-1/4V^2$. The estimation procedure of the reflection profile beneath the site using the auto-covariance function of surface recordings under the assumption of a stationary process was developed by Claerbout (1968), and this procedure is currently being developing as the seismic interferometry method. The difference between one-dimensional seismic interferometry and the proposed method is described later herein.

As described in the preceding discussion, the up-coming and down-going waves of shearing strain generate constructive interference at layer boundaries for the shearing wave that propagates into a higher-velocity layer, and thus the local maxima of instantaneous power are produced. Therefore, given that the surface velocity recordings are modulated by the response of multi-layered media, the characteristics of the instantaneous power of the strain wave $\varepsilon(t, h)$ must be derived from surface velocity recordings only, the characteristics of which show the local maxima at lag times in relation to the depth time of the layer boundaries. Here, the shearing strain wave normalized by $1/2V$ must be considered as follows:

$$x^{(-)}(t, h) \equiv v\left(t + \frac{h}{V}\right) - v\left(t - \frac{h}{V}\right). \quad (14)$$

The wave $x^{(-)}(t, h)$ is hereinafter referred to simply as the strain wave. The strain wave corresponds to $\{x_n^{(-)}(k\Delta T)\}$ in the left-hand side of relation (7), and, thus, the instantaneous power is given by

$$\left|x^{(-)}(t, h)\right|^2 = R\left(t + \frac{h}{V}, 0\right) + R\left(t - \frac{h}{V}, 0\right) - R(t, \tau) - R^*(t, \tau). \quad (15)$$

The instantaneous auto-covariance function $R(t, \tau)$ in the right-hand side of relation (15) is defined as follows:

$$R(t, \tau) \equiv v\left(t + \frac{\tau}{2}\right) v^*\left(t - \frac{\tau}{2}\right), \quad \tau = \frac{2h}{V}, \quad (16)$$

and $R(t, \tau)$ satisfies Hermitian symmetry:

$$R^*(t, -\tau) = R(t, \tau).$$

Relations (15) and (16) indicate that the instantaneous power of the strain wave associated with the rays at a depth of h is represented by the instantaneous auto-covariance function of surface velocity recordings with different time origins, t and $t \pm h/V$, and the lag-time τ is translated from depth h, assuming that the velocity V is constant.

At this point, the difference between one-dimensional seismic interferometry (Claerbout, 1968; Nakahara, 2006) and the proposed method may be clear, although both methods are constructed based on the auto-covariance function of surface seismograms. In the seismic interferometry, assuming the second-order stationary process of surface recordings, the auto-covariance function of surface recordings, $R_V(\tau)$, is approximately expanded as follows:

$$R_V(\tau) = \int R_I(\xi) R_H(\tau - \xi) d\xi \approx \int_0^{T_I} R_I(\xi) d\xi \cdot R_H(\tau) \quad \text{for } \tau > T_I, \quad (17)$$

where $R_I(\xi)$ and $R_H(\xi)$ are the auto-covariance function of the input wave for a sedimentary layer-basement system and that of the impulse response of the system, respectively. This approximation is based on the following assumptions: $R_I(\xi) \approx 0$ for $\xi \geq T_I$ and $R_I(\tau) \approx R_I(\tau + T_I)$ for any $\tau > T_I$. Seismic interferometry estimates the reflection profile of a sedimentary layer-basement system from $R_V(\tau) \approx$ constant $\cdot\, R_H(\tau)$ for $\tau > T_I$, and thus the azimuth average of the depths of velocity discontinuities in the system is estimated. Clearly, the concept of lapse time no longer exits. The auto-covariance function used in the proposed method is given by relation (16) and is a function of two time variables, lapse time t and delay time τ. The basic relation used to detect velocity boundaries in a sedimentary layer-basement system, i.e., relation (15), retains two time parameters in the auto-covariance function of surface recordings. This nonstationarity is essential in the present study. In the nonstationary ray decomposition, the local maxima of the instantaneous power of the strain wave vary with the lapse time and depth time depending on the instantaneous auto-covariance function. Thus, for example, it is possible to detect a series of depth times for seismograms containing a sequence of totally reflected pulses generated at the upper boundary of the dipping basement (Kinoshita, 1985).

Similar to relation (7), relation (15) is calculated in terms of the Wigner-Ville distribution. The Wigner-Ville distribution is defined by the Fourier transform of the instantaneous auto-covariance function given by relation (16), as follows:

$$W(t, f) = \int_{-\infty}^{\infty} R(t, \tau) e^{-i2\pi f \tau} d\tau \tag{18}$$

Conversely, the inverse Fourier transform is as follows:

$$R(t, \tau) = \int_{-\infty}^{\infty} W(t, f) e^{i2\pi f \tau} df \tag{19}$$

In relation (19), $\tau = 0$ yields

$$R(t, 0) = \int_{-\infty}^{\infty} W(t, f) df \tag{20}$$

Thus, using relations (19) and (20), relation (15) is rewritten as

$$\left|x^{(-)}(t, h)\right|^2 = \int_{-\infty}^{\infty} \left[W\left(t + \frac{h}{V}, f\right) + W\left(t - \frac{h}{V}, f\right) - 2W(t, f) \cos\left(2\pi f \cdot \frac{2h}{V}\right) \right] df \geq 0. \tag{21}$$

Using the following notation,

$$R_{x(-)}(t, \tau = 0; h) \equiv x^{(-)}\left(t + \frac{\tau}{2}, h\right) \cdot x^{(-)*}\left(t - \frac{\tau}{2}, h\right)\Big|_{\tau=0} \tag{22}$$

in the left-hand side of relation (21), relation (21) is rewritten as

$$\int_{-\infty}^{\infty} W_{x(-)}(t, f; h)\, df = \int_{-\infty}^{\infty} \left[W\left(t + \frac{h}{V}, f\right) + W\left(t - \frac{h}{V}, f\right) - 2W(t, f) \cos\left(2\pi f \cdot \frac{2h}{V}\right) \right] df. \tag{23}$$

Trivially, the following equation is satisfied:

$$R_{x(-)}(t, 0; h) = \int_{-\infty}^{\infty} W_{x(-)}(t, f; h)\, df. \tag{24}$$

Relation (23) is written in the domain of the Wigner-Ville distribution as

$$W_{x(-)}(t, f; h) = W\left(t + \frac{h}{V}, f\right) + W\left(t - \frac{h}{V}, f\right) - 2W(t, f) \cos\left(2\pi f \cdot \frac{2h}{V}\right). \tag{25}$$

Relation (25) in terms of the Wigner-Ville distribution is related to relation (21) by the instantaneous auto-covariance function, and so retains the physical interpretation of relation (21). Namely, the left-hand side of relation (25) is the Wigner-Ville distribution of the strain wave associated with the ray at time t and depth h, and the right-hand side is composed of three Wigner-Ville distributions of the velocity wave recorded at the surface at times t and $t \pm h/V$. Thus, using relation (25), the distribution $W_{x(-)}(t, f; h)$ of the strain wave associated with the rays is obtained for a variable depth of h. Hence, the following equation is satisfied at $h = 0$, i.e., at the surface:

$$W_{x(-)}(t, f; h = 0) = 0. \tag{26}$$

In the calculation of relations (23) and (25), a common two-way time of each layer ΔT for an equal-time layered model is explicitly contained in these equations by setting $h/V = n \cdot \Delta T$, $n = 0, 1, 2, \ldots$ The parameter ΔT also functions as the sampling time of surface velocity recordings. As a result, relation (21) or (23) is the (t, τ)-representation of the ray, i.e., the instantaneous power of the strain wave $x^{(-)}(t, h)$ estimated using surface velocity recordings only.

2.3 Basic characteristics of nonstationary ray decomposition

Finally, we consider the applicability range of the instantaneous power to be estimated by relation (21) using surface velocity recordings for a homogeneous half space to the instantaneous power given by relation (7) for a multi-layered model. The following two basic characteristics are plainly acceptable:

(1) The lapse time t and depth time τ are both real times. This means that the actual slopes are $+1$ and -1 for up-coming and down-going rays, respectively, in the (t, τ) space. This feature is satisfied both for the equal-time layered model and the homogeneous half space model. Thus, the instantaneous powers given by relations (7) and (21) are associated with the rays of a straight course. The intersections of two rays with $+1$ and -1 slopes in the (t, τ) space involve possible velocity boundaries, although they are virtual boundaries in the homogeneous half space model.

(2) The instantaneous power of the strain wave $x^{(-)}(t, \tau)$ has local maxima at the velocity boundary, i.e., the intersection of up-coming and down-going rays for the equal-time layered model. Since the local maxima in the (t, τ) space are due to the constructive interference of the strain wave (strictly speaking, the wave of which the half-wavelength must be less than the boundary depth, as discussed later herein), the depth times showing local maxima are preserved for the homogeneous half space model, except for the discontinuity of the instantaneous power of $x^{(-)}(t, \tau)$ at the velocity boundaries in the equal time layered model. Hence, nonstationary ray decomposition using relation (21) can be used to detect the velocity boundaries in the equal-time layered model by finding the local maxima of $x^{(-)}(t, \tau)$, if the local maxima are located at the intersection of up-coming and down-going rays in the (t, τ) space for the homogeneous half space model.

These two basic characteristics reveal that the application of nonstationary ray decomposition to the estimation of velocity boundaries in a layered structure is possible.

3. Estimation of the Velocity Boundaries of the Sedimentary Layer-Basement System

As an application of nonstationary ray decomposition, the velocity boundaries of a sedimentary layer-basement system at two Kanto sediment stations, the FCH (Fuchu)

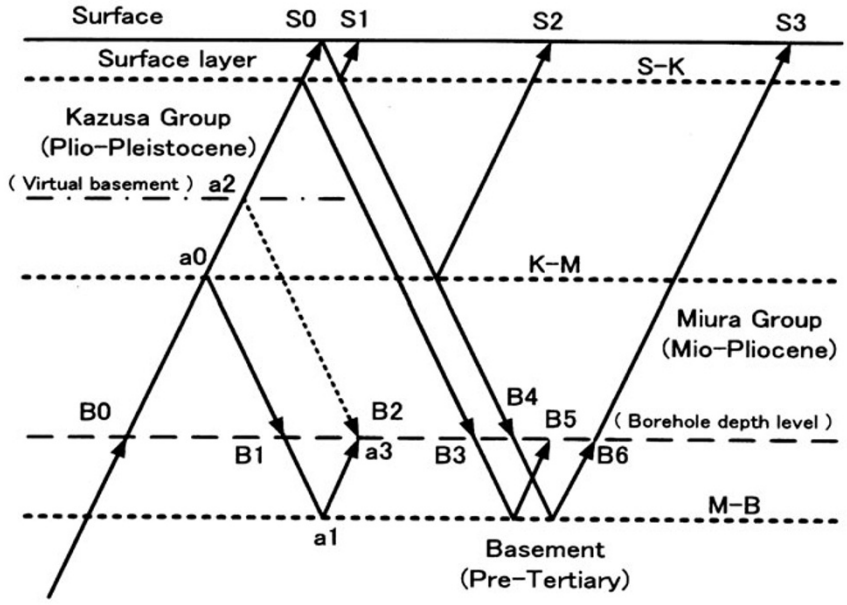

Fig. 4. Model structure used for the investigation of velocity structures beneath the FCH and YKH sites.

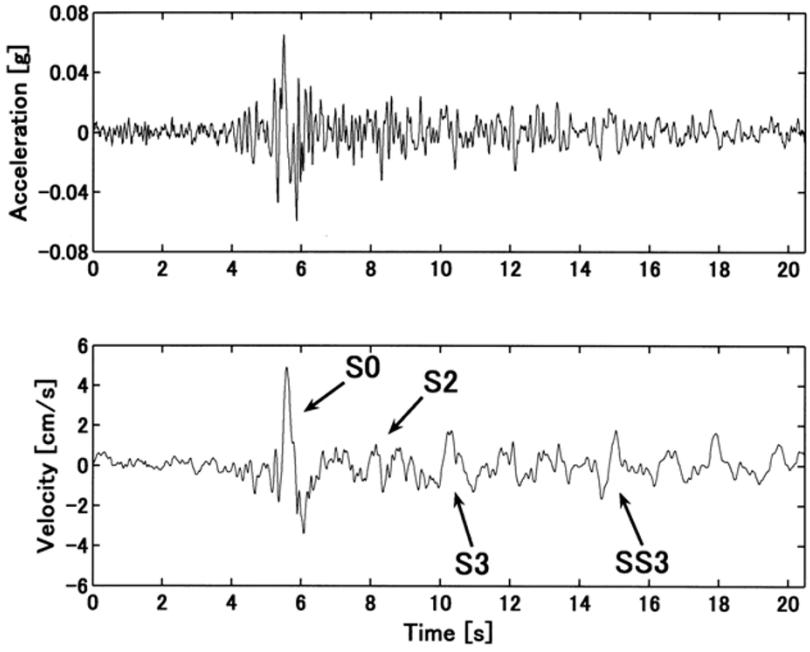

Fig. 5. Transverse component of surface recordings obtained at the FCH site for the earthquake of September 25, 1980 (M 6.1): (top) acceleration and (bottom) velocity waves.

and YKH (Yokohama) stations in Japan are estimated using strong-motion recordings obtained at the surface. The YKH site is the same as the KNGH10 site of KiK-net (Okada *et al*., 2004). The velocity structure at the FCH site was obtained by the down-hole method (Yamamizu *et al*., 1980) to a depth of 2.75 km, and that of the YKH site was also examined by the well VSP method to a depth of 2 km (Yamamizu, 2004). The depth level of the top of pre-Tertiary basement is 2 km at the FCH site. In contrast, the depth level of the basement at the YKH site is unknown, but is deeper than 2 km. Surface acceleration recordings obtained by a tri-axial accelerometer are used for both sites. In addition to the surface recordings, data recorded by a tri-axial accelerometer installed at a depth of 2 km is also investigated at the YKH site. The tri-axial accelerometer is a negative feedback accelerometer with a natural frequency of 450 Hz and a damping factor of 0.6–0.7. The sensitivity is 3 V/g and the sampling rates are 100 and 200 Hz for the FCH and YKH sites, respectively.

The velocity structure shown in Fig. 4 is used for a com-

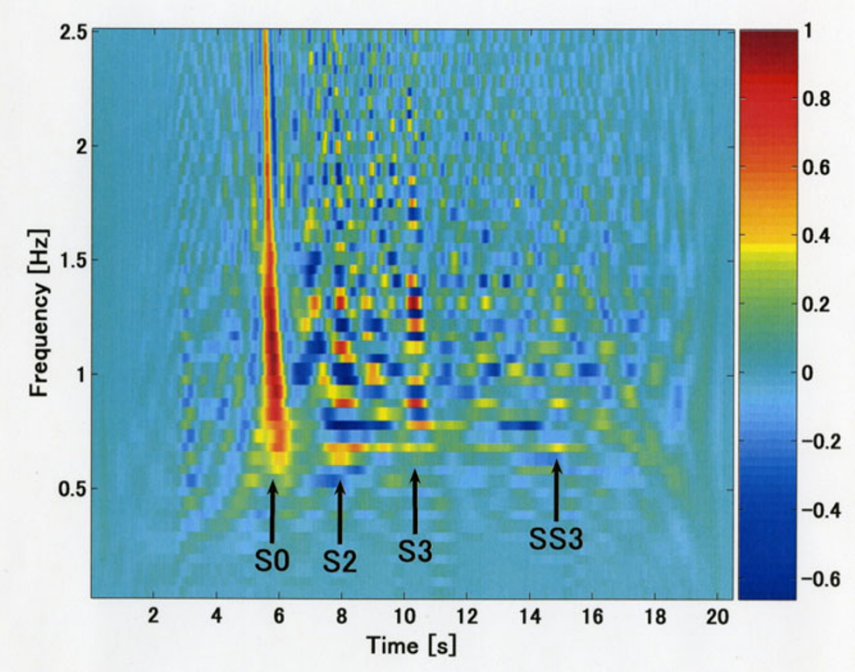

Fig. 6. Wigner-Ville distribution estimated using the velocity data shown at the bottom of Fig. 5.

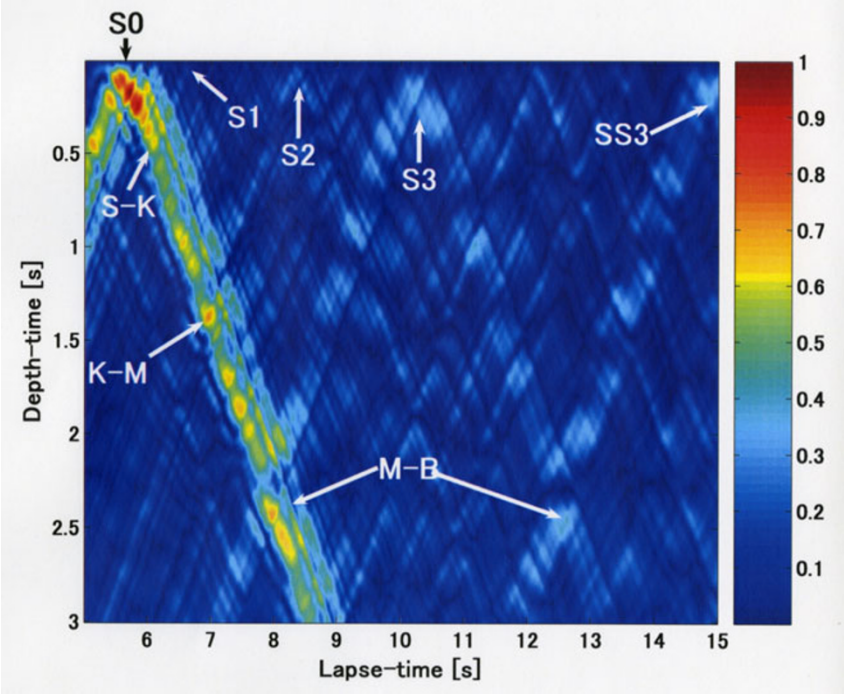

Fig. 7. Normalized root mean square of instantaneous power in the (t, τ) space, estimated using the velocity wave shown at the bottom of Fig. 5.

mon model in this region (Yamamizu *et al*., 1980) and is referred to in the present study. The major velocity boundaries in this model, i.e., the reflection boundaries, are the M-B (Miura group-pre-Tertiary Basement), K-M (Kazusa group-Miura group), and S-K (Surface layer-Kazusa group) boundaries, as labeled in Fig. 4. The real velocity boundaries do not always agree with the geological boundaries, except for the M-B boundary. Thus, these boundary names are simply symbolic names used for convenience. The mean S-wave velocities are 0.7, 1.2, and 2.5 km/s for the Kazusa group, Miura group, and pre-Tertiary basement, respectively, as estimated by Yamamizu *et al*. (1980).

3.1 FCH site

The first site for applying non-stationary ray decomposition to the estimation of velocity boundaries is the FCH site (35.6507N, 139.4736E) using strong-motion data for the earthquake of September 25, 1980, ($M = 6.1$) with the epicenter at 35.576N, 140.134E and a focal depth of 71 km. The transverse component waves are shown in Fig. 5. These are the original acceleration (top) and velocity

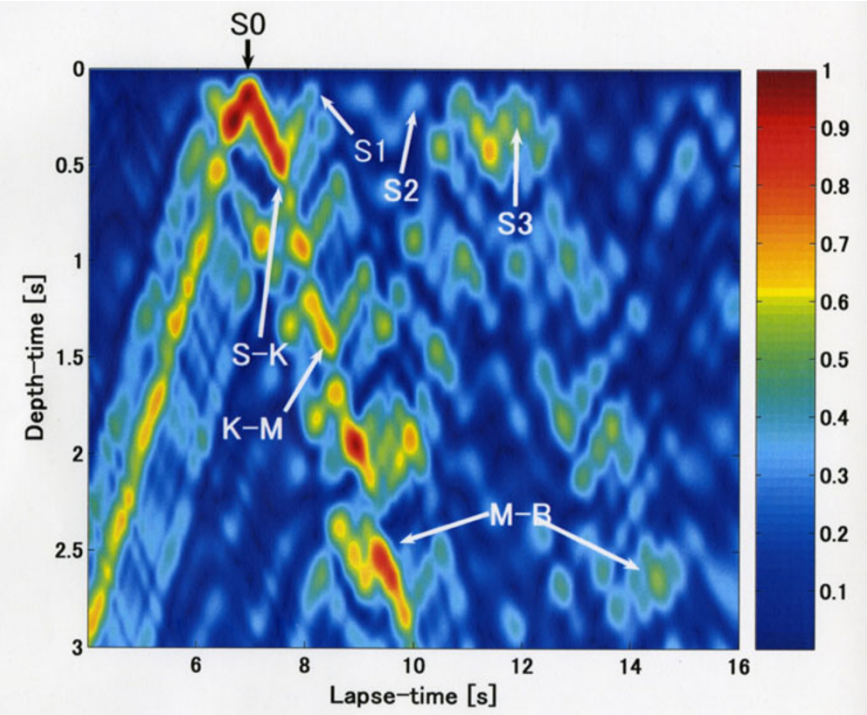

Fig. 8. Normalized root mean square of instantaneous power in the (t, τ) space, estimated using the surface velocity data recorded at the FCH site for the earthquake of July 23, 2005 (M 6.0).

(bottom) waves converted from the acceleration data.

Using the transverse velocity data with a duration of 20.48 s, as shown in Fig. 5, the Wigner-Ville distribution is estimated as shown in Fig. 6. Three energy-concentrated phases are detected at approximately 6, 8.5, and 10.5 s (labeled $S0$, $S2$, and $S3$ in Fig. 6). The first phase is a direct S-wave, and the others phases are reflected phases. Careful observation reveals an isolated phase at approximately 15 s, which is labeled $SS3$. These energy concentration times are in good agreement with the corresponding phases as labeled in Fig. 5.

Figure 7 shows the (t, τ)-representation of the ray estimated by applying relation (21) to the Wigner-Ville distribution shown in Fig. 6. The first finding is most probably the boundary with a depth time of approximately 2.35 s and reflected waves, which are labeled $S3$ and $SS3$, corresponding to two phases around the lapse times of approximately 10.5 and 15 s in Fig. 5. Given the depth time estimated from the equal-time layered structure at the FCH site shown in Fig. 1, this boundary is the M-B boundary. A later phase, labeled $S2$, that appeared at a lapse time of approximately 8.5 s is a reflected phase from the boundary with a depth time of approximately 1.4 s in the (t, τ)-representation of the ray, as shown in Fig. 7. This boundary is the K-M boundary according to the equal-time layered model in Fig. 1. The possible reflected phase, labeled $S1$ in Fig. 7, is a reflected wave at the S-K boundary, although the identification of this phase in Fig. 6 is less clear compared with the $S2$ and $S3$ phases. Clearer detection of the $S1$ phase may require the band-limited wave of the velocity seismogram shown at the bottom of Fig. 5. This is discussed in the Discussion section. However, the results of the (t, τ)-representation of the ray are in good agreement with the velocity structure at the FCH site, as determined by the down-hole method using a 2.75-km deep well (Yamamizu *et al.*, 1980).

Furthermore, in order to verify the results shown in Fig. 7, the results obtained using another seismogram are examined. The seismogram is recorded at the FCH site for the earthquake of July 23, 2005 ($M = 6.0$) with the epicenter at 35.582N, 140.138E and a focal depth of 73 km. The hypocenter and magnitude of this event are approximately identical to those of the event of September 25, 1980. The (t, τ)-representation of the ray obtained from this event is given in Fig. 8. The depth times for the S-K, K-M, and M-B boundaries in Fig. 8 are understood to be in agreement with those in Fig. 7.

3.2 YKH (KNGH10) site

The YKH site (35.4959N, 139.5227E) of KiK-net (Okada *et al.*, 2004) was constructed in 1992. Thus, only the transverse component velocity seismogram recorded at this site for the earthquake of July 23, 2005 ($M = 6.0$) with the epicenter at 35.582N, 140.138E and a focal depth of 73 km is examined. The seismogram is shown at the top of Fig. 9. However, reflected phases on the original velocity wave are masked by the predominant motion of the soft surface layer beneath the site and are difficult to detect without proper preprocessing. Thus, in order to facilitate the detection of the reflected phase, the band-limited wave composed by intrinsic mode functions (Huang *et al.*, 1998), as shown in the bottom of Fig. 9, is used. Hence, the original and band-limited waves, $v(t)$ and $v_o(t)$, are expanded as follows:

$$v(t) \approx \sum_{k=1}^{15} v_k(t) \quad \text{and} \quad v_o(t) = \sum_{k=3}^{7} v_k(t).$$

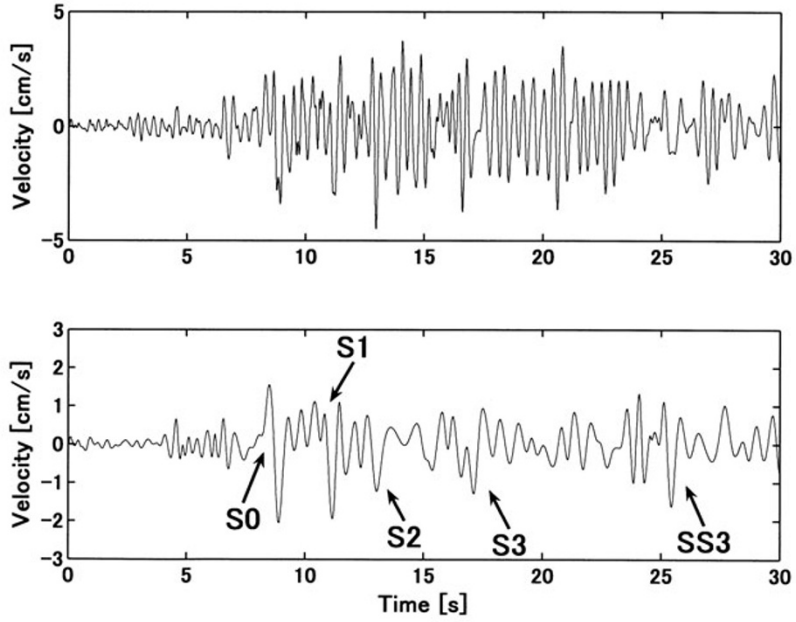

Fig. 9. Transverse component of surface recordings obtained at the YKH site for the earthquake of July 23, 2005 (M 6.0): (top) velocity and (bottom) band-limited velocity waves.

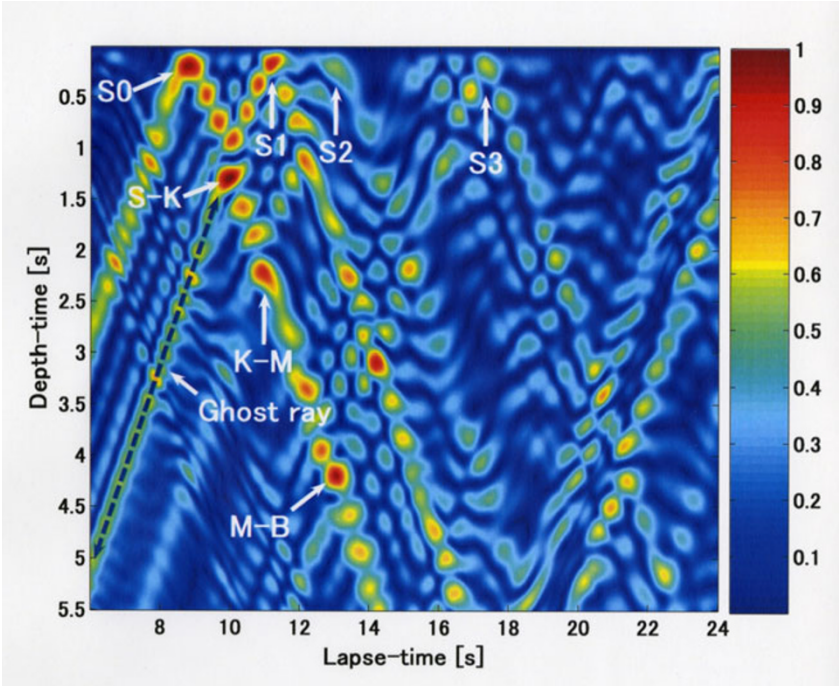

Fig. 10. Normalized root mean square of instantaneous power in the (t, τ) space, estimated using the band-limited velocity wave shown at the bottom of Fig. 9.

Functions $\{v_k(t)\}_{k=1}^{15}$ are the intrinsic mode functions of $v(t)$. This band-pass filtering is an application of the Empirical Mode Decomposition (EMD) method proposed by Huang *et al*. (1998), and the EMD based filtering has superior characteristics for nonstationary seismic waves, i.e., the EMD based filtering is free from the group delay and settling time of seismic phases. Since the method of ray decomposition in the present study is intended to clarify the nonstationarity of the seismic waves associated with rays, such a preprocessing is reasonable. Details for the calculation of intrinsic mode functions and for the applications to the filtering and phase identification problems using strong-motion seismograms are given by Huang *et al*. (1998, 2001) and Kinoshita *et al*. (2009)

The labeling of reflected phases can be achieved by comparing the results of the estimated (t, τ)-representation of the ray shown in Fig. 10 with the band-limited seismogram at the bottom of Fig. 9. The depth time of the basement is

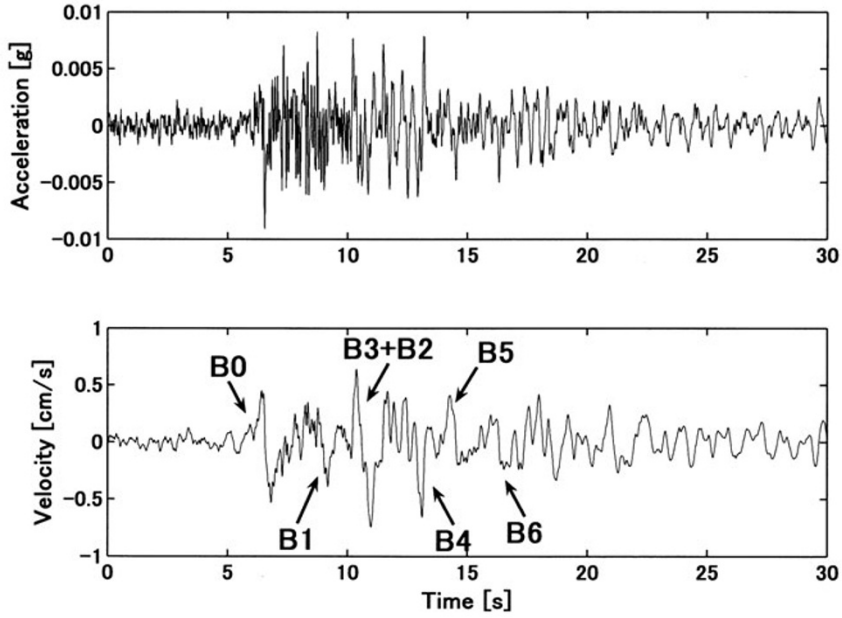

Fig. 11. Transverse component of recordings obtained at a depth of 2 km at the YKH site for the earthquake of July 23, 2005 (M 6.0): (top) original acceleration and (bottom) converted velocity waves.

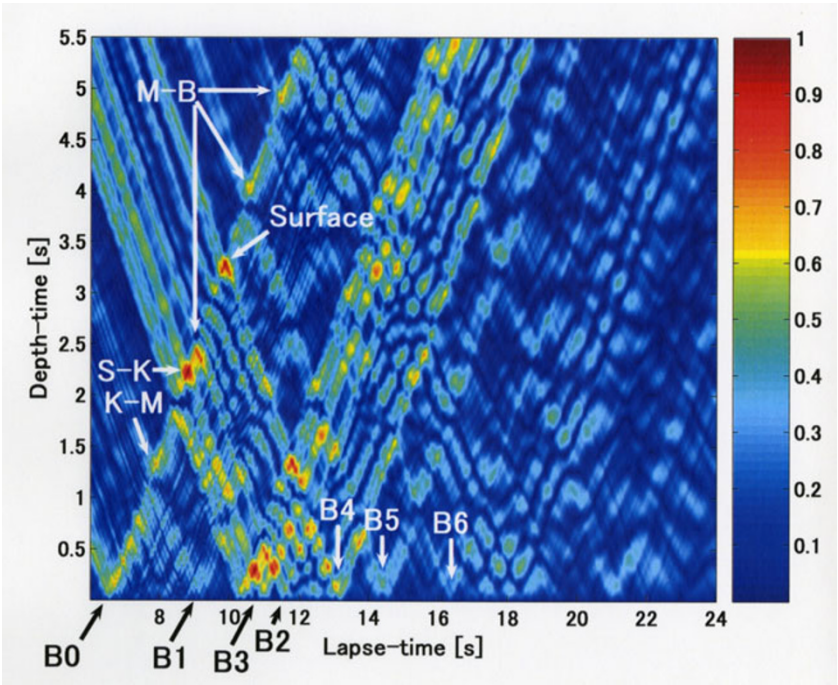

Fig. 12. Normalized root mean square of instantaneous power in the (t, τ) space, estimated using the velocity wave shown at the bottom of Fig. 11.

approximately 4.3 s, and the corresponding reflected phases are labeled $S3$ and $SS3$. The reflected phase $S1$ from a boundary with a depth time of approximately 1.3 s, which was clearly detected by a well VSP method (Yamamizu, 2004) and is labeled as the S-K boundary in this article, is the most conspicuous phase. The reflection boundary of the $S2$ phase might be the K-M boundary, which was unclear (Yamamizu, 2004). Thus, the depth times of the boundaries obtained in the present study are in agreement with the results obtained by Yamamizu (2004).

A tri-axial accelerometer is also installed at a depth of 2 km at the YKH site, so that verification of the results obtained from surface recording is possible, although the interpretation of the (t, τ)-representation of the rays obtained using borehole data is fairly complex. In the case of surface recordings, direct interpretation of the reflected phase from the boundaries in a sedimentary layer-basement system is possible. In contrast, the interpretation of borehole recordings must be taken into consideration for both the downcoming wave from surface, or the boundaries lying over the

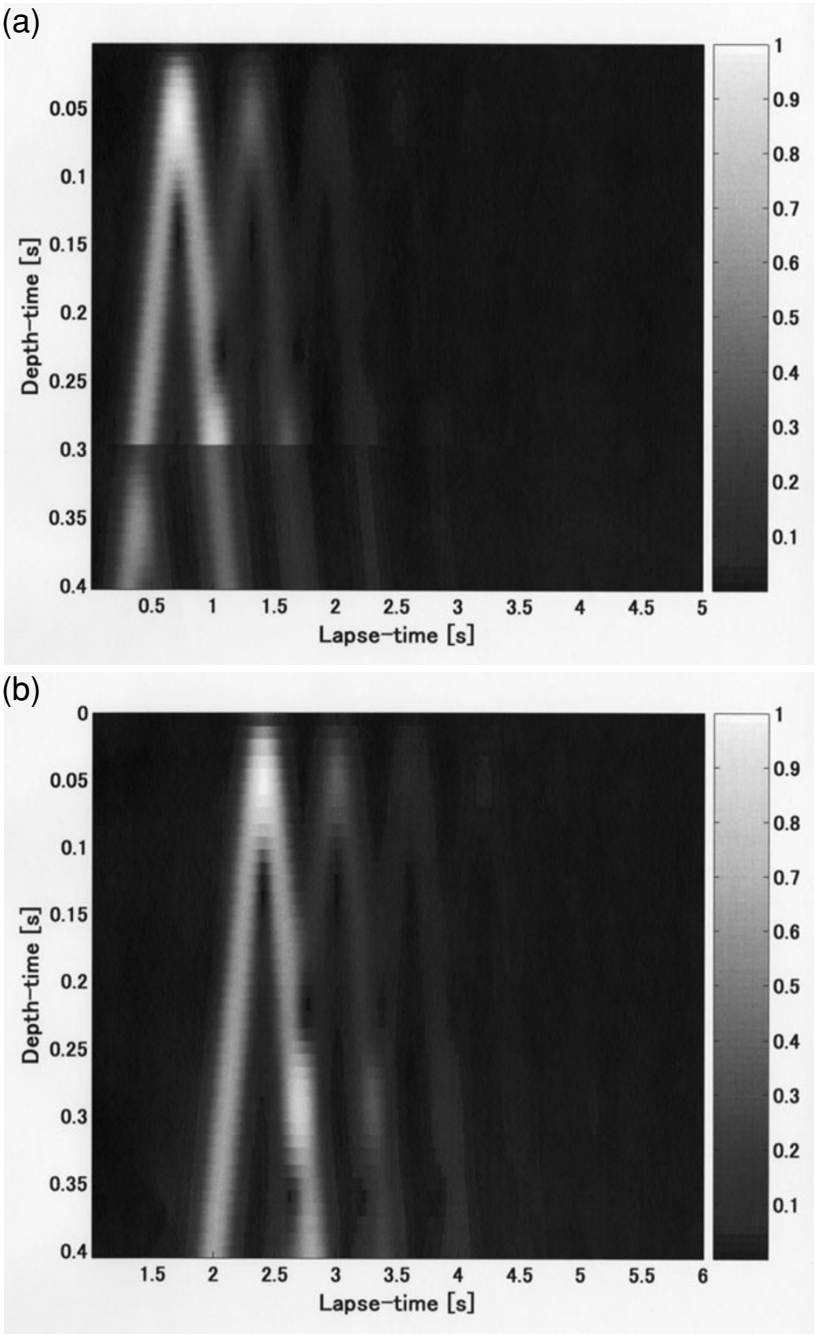

Fig. 13. Normalized root mean square of instantaneous power in the (t, τ) space: (a) calculated results for a layered model and (b) estimated results using the surface output signal for a homogeneous half space model. The layered model consists of a surface layer (S-wave velocity, density and thickness are 0.2 km/s, 1.8 g/cm^3 and 60 m, respectively) overlying a higher velocity half-space (S-wave velocity and density are 0.4 km/s and 2.0 g/cm^3, respectively). The input wave is a Ricker wavelet with a center period of 0.3 s.

borehole depth level, and its up-coming wave reflected at the top of the basement, which is located beneath the depth level of the borehole, as shown in Fig. 4. Thus, the depth time of the basement from the surface or the boundaries is obtained by summing the depth time of the re-reflected phase from the top of the basement and the depth time of the boundary located over the depth level of the borehole along the same ray in the (t, τ)-representation. For example, the depth time of the B2 phase in Fig. 4 is obtained by considering a path from a0 to a3 via a2, instead of a path from a0 to a3 via a1, forming a virtual basement over the K-M boundary, as indicated by a dash-dotted line. This task requires trial and error. As a result, the labeling of reflected phases and boundaries, as shown in Figs. 11 and 12, may be most possible, according to the sedimentary layer-basement system modeled in Fig. 4. This result is in good agreement with the depth times of boundaries in the sedimentary layer-basement shown in Fig. 10, which is obtained from surface recording.

4. Discussion

Nonstationary ray decomposition provides a method for estimating velocity boundaries in a sedimentary layer-basement system. In this method, the depth-dependent

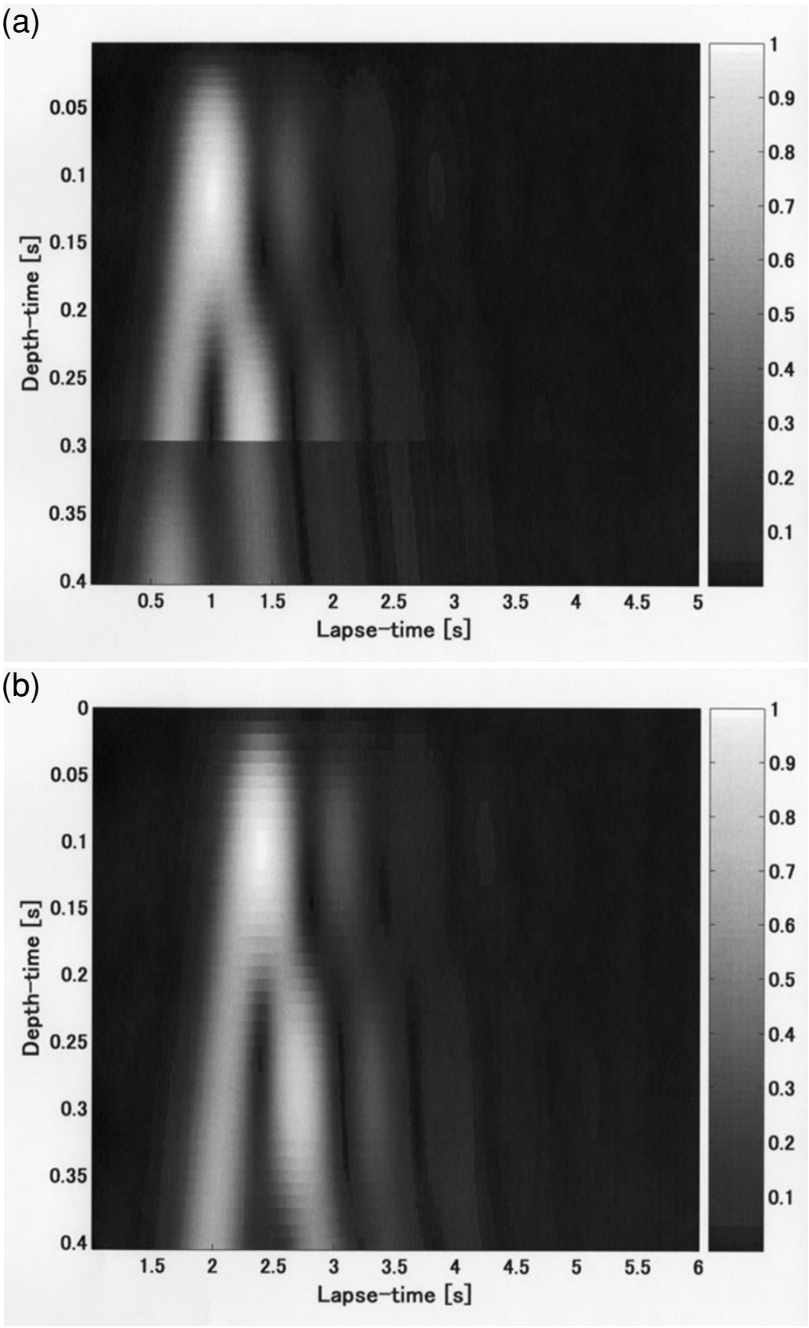

Fig. 14. Normalized root mean square of instantaneous power in the (t, τ) space: (a) calculated results for a layered model and (b) estimated results using the surface output signal for a homogeneous half space model. The layered model is the same model used in Fig. 13. The input wave is a Ricker wavelet with a center period of 0.6 s.

profile of the instantaneous power of the strain wave for a real sedimentary layer-basement system is homologized with the profile in the (t, τ)-representation of the ray in the homogeneous half space model. However, this correspondence of instantaneous power is not identical, as discussed in the Method section. Consider the restrictions imposed on the application of non-stationary ray decomposition to the detection of layer boundaries, i.e., how the frequency band of surface recordings used in the nonstationary ray decomposition is limited. Assume that nonstationary ray decomposition is applied to the boundary detection of a single sedimentary layer overlying the pre-Tertiary basement. An upper frequency limit is derived from the coherency characteristics of the seismic wave traveling in a sedimentary layer-basement system. Kinoshita and Ohike (2006) showed that the upper frequency limit of coherent propagation for seismic waves is approximately 3 and 6 Hz for S- and P-waves, respectively. Thus, a frequency of approximate 3 Hz might be a guideline for the upper frequency of the SH-wave used to estimate the depth time of the top of the basement.

On the other hand, the lower frequency limit could be obtained from the difference in instantaneous powers of the strain wave obtained for a layered model and the strain wave obtained for a homogeneous half space model. Namely, the instantaneous power of the strain wave in the (t, τ)-representation of ray for the layered structure shows dis-

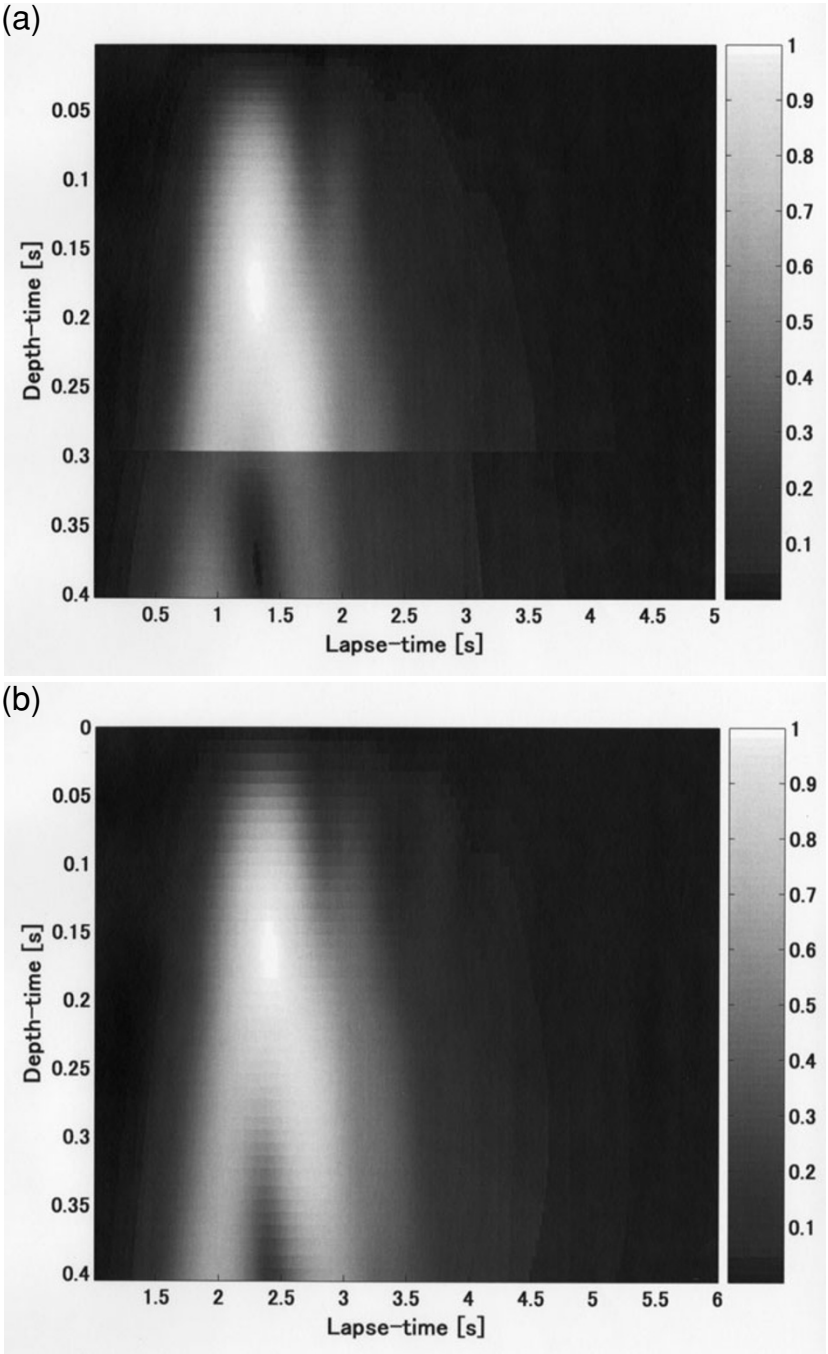

Fig. 15. Normalized root mean square of instantaneous power in the (t, τ) space: (a) calculated results for a layered model and (b) estimated results using the surface output signal for a homogeneous half space model. The layered model is the same model used in Fig. 13. The input wave is a Ricker wavelet with a center period of 0.9 s.

continuity at layer boundaries, although the instantaneous power is a continuous function of depth time and shows only local maxima for the homogeneous half space. Thus, a required limit for lower frequency is obtained from the condition in which the local maxima of instantaneous power remain at the depth time of the velocity boundary. This condition could be clarified by a straightforward simulation. Consider a model with a surface layer overlying a higher velocity half space and a homogeneous half space model. For both models, the results shown in Figs. 13, 14, and 15 are obtained for Ricker wavelet inputs with center periods of $T_o = 0.3$, 0.6, and 0.9 s, respectively. Suffixes "a" and "b" attached to each figure number indicate simulations performed for the layered model and for the homogeneous half space model, respectively. The local maximum of the instantaneous power of the strain wave is found at a depth time of $\tau_o = 0.3$ s under the input of the Ricker wavelet with the center periods of $T_o = 0.3$ and 0.6 s for both models. However, for $T_o = 0.9$ s, the layer boundary in Fig. 15(a) is detectable using the discontinuity of instantaneous power, but is difficult to determine from the local maximum of instantaneous power in Fig. 15(b). These results indicate that the maximum instantaneous power at $\tau_o = 0.3$ s is discriminated under the period condition of $T_o \leq 2\tau_o$. In contrast,

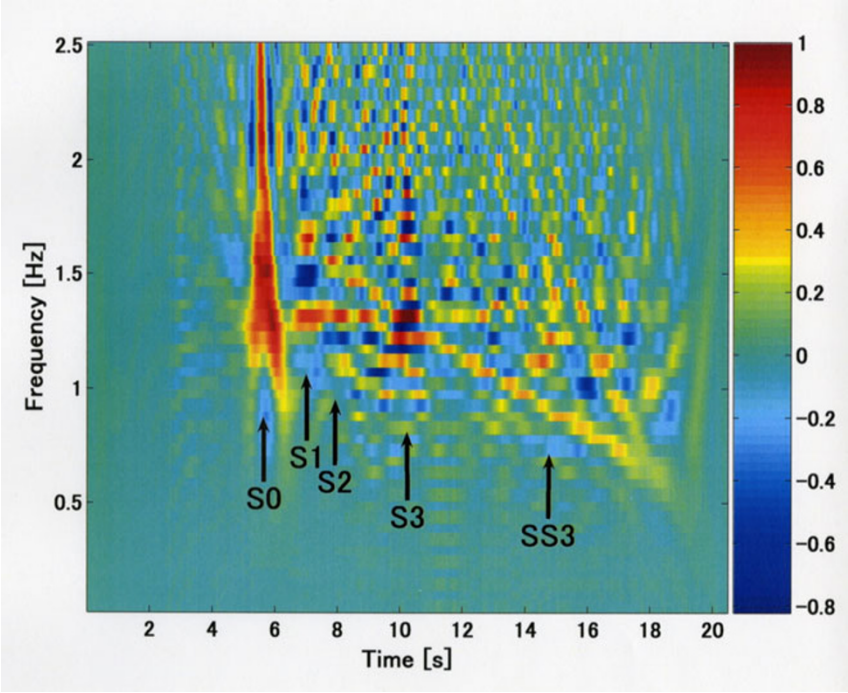

Fig. 16. Wigner-Ville distribution estimated using the high-pass-filtered velocity seismogram filtered with a cutoff frequency of approximately 1 Hz.

for $T_o = 3\tau_o$, the discrimination of the maximum instantaneous power at $\tau_o = 0.3$ s is difficult. This means that the half wavelength of the Ricker wavelet with a center period of τ_o determines the lower frequency limit. Hence, the reasonable frequency band of the *SH*-wave used for estimation of the layer boundary with a depth time of τ_o in a sedimentary layer-basement system is $1/2\tau_o \leq f \leq 3$ Hz. This means that for the estimation of a layer boundary with a large depth time, seismic waves having low-frequency components can be used. For example, seismic waves with a frequency band of $1/2\tau_o \approx 0.1 \leq f \leq 3$ Hz can be used to determine the boundary of the top of the pre-Tertiary basement at the YKH site, because the depth time at the boundary between the sedimentary deposit and the basement at this site is approximately 4.5 s, as shown in the preceding investigation.

This result can also be applied to the detection of $S1$ phase for the first example in Section 3.1, where the seismogram recorded at the FCH site for the earthquake of September 25, 1980 is examined. The resultant (t, τ)-representation of the ray shows that the depth time of the S-K boundary is $\tau_o \approx 0.5$ s. Thus, wave components with periods longer than $2\tau_o \approx 1$ s are not needed for the detection of $S1$ phase. The Wigner-Ville distribution recalculated using the high-pass filtered wave decayed the wave components with periods of longer than 1 s, as shown in Fig. 16. The $S1$ phase is clearly discriminated in Fig. 16, as compared to the same phase in Fig. 6, which was obtained using the original seismogram without any filtering.

Finally, as is common with such methods, nonstationary ray decomposition generates ghost rays, as indicated by the dashed black line in Fig. 10, because the decomposition forces a seismic phase on surface recordings to wave power associated with up-coming and down-going rays.

5. Conclusions

The present article demonstrated a method based on nonstationary ray decomposition that decomposes the *SH*-wave at the surface into the instantaneous power of the shearing strain associated with rays in a homogeneous half space as a function of lapse time t and depth time τ, which is the travel time for the depth direction. By applying this method to strong motion data recorded at the FCH and YKH sites in the Kanto district, the following results were obtained:

(1) The method of nonstationary ray decomposition indicates that the velocity boundaries in a sedimentary layer-basement system, whose information is involved in surface recordings, are represented by the local maxima at the intersections of up-coming and down-going rays in the (t, τ) space.

(2) The method of nonstationary ray decomposition was applied to surface recordings at the FCH site, so that the estimated velocity boundaries are in good agreement with the major boundaries in a sedimentary layer-basement system at the site, which were previously estimated using the down-hole method. At the YKH site, a major velocity boundary in the sedimentary deposit was detected, the boundary of which agreed with a boundary previously estimated by the seismic VSP method. The depth time of the boundary between the sedimentary layer and pre-Tertiary basement beneath the YKH site was determined using surface and 2,000-m borehole data separately.

(3) A reasonable frequency band of *SH*-waves used for the estimation of the boundary with a depth time of τ_o is $1/2\tau_o \leq f \leq 3$ Hz. The upper limit of the frequency band is due to the upper-limited frequency of the coherent propagation of *SH*-waves in a sedimentary layer-basement system in the Kanto district.

(4) The instantaneous power of the shearing strain estimated by this method is a continuous function of depth time, and ghost rays are generated in the (t, τ)-representation of the ray.

Acknowledgments. The author would like to thank Hisashi Nakahara for his valuable suggestions and critical comments. Comments from the two anonymous reviewers were also helpful in improving the manuscript. Thanks are also due to the National Research Institute for Earth Science and Disaster Prevention (NIED) for providing the strong motion records at the FCH and YKH sites. This work was partly supported by JSPS Grant-in-Aid for Scientific Research C 20540413.

References

Claasen, T. A. C. M. and W. F. G. Mecklenbrauker, The Wigner distribution—A tool for time-frequency signal analysis. Part I: Continuous-time signals, *Philips J. Res.*, **35**, 217–250, 1980a.

Claasen, T. A. C. M. and W. F. G. Mecklenbrauker, The Wigner distribution—A tool for time-frequency signal analysis. Part II: Discrete-time signals, *Philips J. Res.*, **35**, 276–300, 1980b.

Claerbout, J., Synthesis of a layered medium from its acoustic transmission response, *Geophysics*, **33**, 264–269, 1968.

Goupillaud, P., An approach to inverse filtering of near surface layer effects from seismic records, *Geophysics*, **25**, 754–760, 1961.

Huang, N. E., Z. Shen, S. R. Long, M. C. Wu, H. H. Shin, Q. Zheng, N. Yen, C. C. Tung, and H. H. Liu, The empirical mode decomposition and Hilbert spectrum for nonlinear and non-stationary time series analysis, *Proc. R. Soc. Lond.*, **A454**, 903–995, 1998.

Huang, N. E., C. C. Chen, K. Huang, L. W. Salvino, S. R. Long, and K. L. Fan, A new spectral representation of earthquake data: Hilbert spectral analysis of Station TCU129, Chi-Chi, Taiwan, 21 September 1999, *Bull. Seismol. Soc. Am.*, **91**, 1310–1338, 2001.

Kinoshita, S., A statistical method for the estimation of wave transfer function, *Proc. JSCA*, **313**, 1–11,1981 (in Japanese).

Kinoshita, S., Propagation of total reflected plane SH pulses in a dipping layer, *Zisin*, **38**, 597–608, 1985 (in Japanese).

Kinoshita, S., A stochastic method for investigating site effects by means of a borehole array—SH and Love waves, *Bull. Seismol. Soc. Am.*, **89**, 484–500, 1999.

Kinoshita, S., Deep-borehole-measured Qp and Qs attenuation for two Kanto sediment layer site, *Bull. Seismol. Soc. Am.*, **98**, 463–468, 2008a.

Kinoshita, S., Tilt measurement using broadband velocity seismograms, *Bull. Seismol. Soc. Am.*, **98**, 1887–1897, 2008b.

Kinoshita, S. and M. Ohike, Coherency characteristics of body waves traveling in a sedimentary layer—basement system in the Kanto region, Japan, *Bull. Seismol. Soc. Am.*, **96**, 165–175, 2006.

Kinoshita, S., H. Ishikawa, and T. Satoh, Tilt motions recorded at two WISE sites for the 2003 Tokachi-Oki earthquake (M8.3), *Bull. Seismol. Soc. Am.*, **99**, 1251–1260, 2009.

Kobori, T. and R. Minai, One-dimensional wave-transfer functions of linear visco-elastic multi-layered half-space, *Bull. Disas. Prev. Res. Inst., Kyoto Univ.*, **18**, 27–64, 1969.

Levinson, N., The Wiener RMS error criterion in filter design and prediction, *J. Math. Phys.*, **25**, 261–278, 1947.

Nakahara, H., Theoretical background of retrieving Green's function by cross-correlation: one-dimensional case, *Geophys. J. Int.*, **165**, 719–728, 2006.

Okada, Y., K. Kasahara, S. Hori, K. Obara, S. Sekiguchi, H. Fujiwara, and S. Aoi, Recent progress of seismic observation networks in Japan—Hi-net, F-net, K-NET and KiK-net—, *Earh Planets Space*, **56**, xv–xxviii, 2004.

Yamamizu, F., Seismic wave velocity structures in Kanto area as revealed by the crustal activity observation well VSP, *Technical note of the National Research Institute for Earth Science and Disaster Prevention*, **251**, 1–75, 2004 (in Japanese).

Yamamizu, F., H. Takahashi, N. Goto, and Y. Ohta, Shear wave velocities in deep soil deposits. Part 3, *Zisin*, **34**, 465–479, 1980 (in Japanese).

S. Kinoshita (e-mail: kkk001@yokohama-cu.ac.jp)